

## Nonlinear dynamic analysis of a quarter vehicle system with external periodic excitation



Shihua Zhou, Guiqiu Song\*, Mengnan Sun, Zhaohui Ren

School of Mechanical Engineering & Automation, Northeastern University, Shenyang, 110819 Liaoning, People's Republic of China

### ARTICLE INFO

#### Article history:

Received 16 October 2015

Received in revised form

26 April 2016

Accepted 26 April 2016

Available online 27 April 2016

#### Keywords:

Vehicle model

Suspension system

Incremental harmonic balance method

Nonlinear dynamics

### ABSTRACT

In this paper, a nonlinear dynamic model of a quarter vehicle with nonlinear spring and damping is established. The dynamic characteristics of the vehicle system with external periodic excitation are theoretically investigated by the incremental harmonic balance method and Newmark method, and the accuracy of the incremental harmonic balance method is verified by comparing with the result of Newmark method. The influences of the damping coefficient, excitation amplitude and excitation frequency on the dynamic responses are analyzed. The results show that the vibration behaviors of the vehicle system can be controlled by adjusting appropriately system parameters with the damping coefficient, excitation amplitude and excitation frequency. The multi-valued properties, spur-harmonic response and hardening type nonlinear behavior are revealed in the presented amplitude-frequency curves. With the changing parameters, the transformation of chaotic motion, quasi-periodic motion and periodic motion is also observed. The conclusions can provide some available evidences for the design and improvement of the vehicle system.

© 2016 Elsevier Ltd. All rights reserved.

### 1. Introduction

The vehicle dynamics plays an important role in the development of vehicle industry, and the vibration [1] and noise of vehicle system caused by external excitation is still a subject of research. The vehicle system is a strong nonlinear system interactions among suspension, tires and other components, which may become uncontrollability and instability caused by the vibration and impact. In addition, Suspension system, as one of the key components, can absorb the most of energy between the tire and vehicle body. Thus, it is important to analyze the dynamic behaviors of the vehicle system. The vehicle system is a typically complicated multi-body nonlinear system, and the nonlinearity degree can be embodied via the number of degree of freedom (DOF) with the established model. Several models have been developed by the researches related to the dynamic behavior of vehicle system [2]. The 2-DOF/1-DOF model (quarter-car model) is used for analyzing the vertical vibration of the body, the 4-DOF model (half-car model) with two-wheel (front and rear, left and right) for studying the vertical and pitch motions, and the 7-DOF full 3-D vehicle model (full-vehicle model) as a four-wheel model for investigating the vertical, pitch and roll motions.

With the increasing demand for high comfort and high safety,

the dynamic behaviors of vehicle system have been extensively studied in the past years, Liang [3] established a 2-DOF nonlinear vehicle suspension model, and analyzed the chaotic behavior of the vehicle passing the consecutive speed control humps on a highway with different parameters. A quarter vehicle system with nonlinear spring and damper was analyzed by Liu [4], which investigateded the effects of the consecutive speed control humps on the dynamic behaviors of the vehicle passing the consecutive speed control humps. Zheng [5] discussed the dynamic responses of a 2-DOF nonlinear suspension system and the chaotic motion could be controlled by using state variable feedback. Li [6] presented a vehicle suspension system with hysteretic nonlinearity and the chaotic motion was derived by the Melnikov function [7], which was subjected to the multi-frequency excitation from road surface. Litak [8–9] used the Melnikov criterion to examine a global homoclinic bifurcation and transition to chaos in the case of a SDOF (single degree of freedom) car model excited kinematically by a road surface profile consisting of harmonic and noisy components. Zhu investigated the dynamic responses of 4-DOF [10] and 7-DOF [11] ground vehicle model, and the disturbances from the road were assumed to be sinusoidal. The results showed that the chaotic response may appear in the unstable region of frequency response diagram. Zhu [12] studied the nonlinear dynamics of a 2-DOF vibration system with nonlinear damping and nonlinear spring, and the amplitude and vibration can be reduced by adjusting properly system parameters and considering the value of excitation frequency. Ikenaga [13] developed a full-vehicle

\* Corresponding author.

E-mail address: [guiqiusong@126.com](mailto:guiqiusong@126.com) (G. Song).

suspension system with an active suspension control approach combining a filtered feedback control scheme and an input decoupling transformation. Zhang [14] proposed a semi-active sliding mode controller based magneto-rheological quarter vehicle suspension through comparing the time and frequency domain responses of the sprung mass and unsprung mass accelerations, suspension travel and the tire dynamic force with those of the passive quarter vehicle suspension, under three kinds of varied amplitude harmonic, rounded pulse and real-road measured random excitations. Borowiec [15] established a SDOF nonlinear model, representing a quarter automobile with semi-active, nonlinear suspension, and the chaotic vibrations and bifurcations of the system were studied with changing excitation frequency and road profile amplitude. Turkay [16] used a quarter-car model to study the response of the vehicle to profile imposed excitation with randomly varying traverse velocity and variable vehicle forward velocity. In addition, root-mean-square responses of the vehicle to white and colored noise velocity road inputs were analyzed. Wagner [17] presented a quarter-car model with nonlinear damping, which was subjected to white or colored noise excitation by using high-dimensional probability density functions. Wu [18] reviewed on the application of chaos theory in automobile nonlinear system, which indicated that the automobile nonlinear system had very abundant and complicated dynamic phenomena. Chaos motion could happen even in the simplest single-freedom nonlinear vertical vibration system of automobile. Verros [19] investigated the dynamics of a controlled quarter-car model by applying an appropriate methodology for obtaining exact periodic motions for the case of forced resulting from a road with harmonic profile. Kropáč [20] build two models: a planar model of a personal car with a driver and one passenger, and a planar model of a three-axle truck. The dynamic behaviors were evaluated caused by passing an isolated obstacle and a number of randomly distributed obstacles. Bum [21] proposed multi-body dynamics model of complete vehicle, and investigated the effects of individual and overall design variable uncertainties on the ride comfort uncertainty. Yang [22] established a 7-DOF nonlinear full-vehicle model and then used numerical simulation to analyze chaotic vibration excited by consecutive speed control humps. Yang [23] studied the possibility of chaotic vibration with the 4-DOF half vehicle model under consecutive speed control humps on the highway. Then, a direct variable feedback control was proposed to eliminate the influence of chaos on vehicle nonlinear vibration and how to select proper control parameters was discussed. Shen [24] analyzed the effects of the time delay on the dynamic responses by four semi-active dynamic vibration absorbers and the comparisons between the analytical and the numerical solutions were presented. Eimadany [25–26] developed an integrated investigation of vehicle dynamics, roadway excitations and performance measures in order to study the dynamic behaviors and design of vehicle suspension systems and the consequences of vehicle ride quality. Sheng [27] studied the chaotic motion of the SDOF nonlinear suspension mathematical model under single frequency sine, multi-frequency harmonic and random road excitation, and the dynamic behaviors were analyzed by using central manifold theorem. Safety analysis and the forced vibration characteristic of a SDOF vehicle suspension system with hysteretic nonlinearity characteristic under road quasi-period multi-frequency excitations were carried out by Yu [28]. Zhuang [29] researched a vehicle model with nonlinear suspension spring and hysteretic damping element, which exhibited multiple heteroclinic orbits in the unperturbed system. Zhong [30] and Lu [31] investigated a kinetic model of the piecewise-linear nonlinear suspension system that consists of a dominant spring and an assistant spring, and the topological bifurcation solutions, motion characteristics with different parameters were obtained. Jerrelnd

[32] studied a 2-DOF model of with coupled suspension systems characterized by piecewise-linear stiffness, which indicated that the coupled system had a more irregular behavior with larger motions than the uncoupled suspension system. Hamed [33] analyzed the dynamic behavior of a quarter-car system with 2-DOF, where the tire was modeled as a nonlinear hardening spring and the disturbance of road assumed to be sinusoid. Ren [34] deduced a 2-DOF system with piecewise and smooth nonlinear coupled differential equations, which were calculated by using Shooting-Method. The results showed that the jump phenomenon would happen with road conditions change suddenly or carrying capacity change hugely. Marzbanrad [35] established a quarter-car nonlinear model with nonlinear air spring and nonlinear damper and then studied the possibility of chaotic vibration of this model under consecutive speed control humps on the highway. Borowiec [36] studied the dynamics of a 2-DOF nonlinear oscillator representing a quarter-car model excited by a road roughness profile, which was modeled by means of a harmonic function. Sheng [37] build a nonlinear dynamic model of automobile heave vibration system with 2-DOF based on an analysis of nonlinear spring force and damping force for automotive suspension and tire by the incremental harmonic balance method (IHBM). The IHBM is a very effective method for solving nonlinear problems, but little work is used to analyze the dynamic behavior of vehicle nonlinear system. The key factor of IHBM is the computation of steady state solution with very short time. Meanwhile, it is well designed for system under periodic excitation, which is very fit for the vehicle nonlinear system. Although there are a lot of literatures concerned with the vehicle system, the studies on nonlinear dynamic characteristics of the forced vibration vehicle system based on IHBM are still very limited. So it is important to research the dynamic characteristics influenced by the system parameters based on the IHBM.

The above cited references have presented the vibration characteristics with the suspension system, the disturbances usually come from the changing random road surface and consecutive speed control hump under running vehicle. However, the vehicle system may similarly suffer from the complexity vibration and harshness problem and especially the vibration property of the vehicle system on offload platform. In this study, a SDOF nonlinear vehicle suspension system with external excitation caused by double eccentric shaft vibration exciter is presented, which is used to investigate the nonlinear dynamic behaviors of the vibration system with the deflection of tire and suspension. The differential equation of the vehicle system is calculated using the IHBM and NMM (Newmark method). The dynamic behaviors of the vehicle system are characterized using time domain, frequency domain, phase diagrams, Poincaré maps, bifurcation diagram and frequency-amplitude curves. The influences of the damping coefficient, excitation amplitude and excitation frequency on the dynamic characteristics are studied, which provide to understand the vibration properties of the vehicle system.

The paper is organized into five sections. Section 2 presents the external excitation and the mathematical modeling of a SDOF nonlinear vehicle system. In Section 3, the IHBM is introduced. The dynamic behaviors of the vehicle system are analyzed in Section 4, and discuss the effects of the key parameters. Finally, Section 5 presents some brief conclusions.

## 2. Nonlinear dynamic model of vehicle suspension system

The dynamic behaviors of vehicle suspension system with external excitation require an integrated investigation. In this section, a SDOF vehicle nonlinear dynamic model is established with nonlinear spring and nonlinear damping. And the external

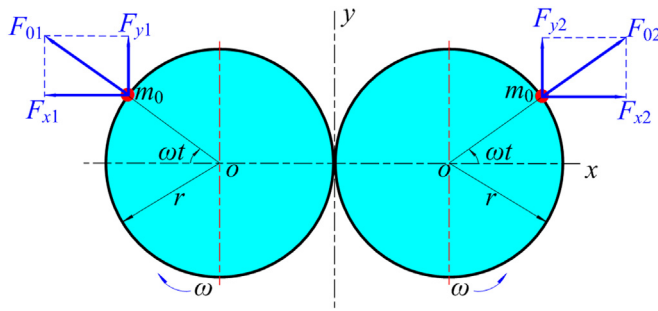


Fig. 1. The external excitation model.

excitation is defined. The differential equation of suspension system is deduced.

### 2.1. The external excitation

The external excitation for the vehicle system is assumed to change in vertical direction caused by double eccentric shaft vibration exciter. The eccentric mass and eccentric distance are the same on double eccentric shaft vibration exciter, which are symmetry in  $y$  direction. When the two shafts are synchronous reverse rotation, the centrifugal forces in  $x$  direction offset each other and the component forces superpose each other in  $y$  direction, which forms a single direction of simple external excitation. The Fig. 1 shows the external excitation model at any moment.

Based on the above analysis, the external excitation in  $y$  direction can be defined as:

$$F = \sum_{i=1}^2 F_{yi} = \sum_{i=1}^2 F_{0i} \sin \omega t = \sum_{i=1}^2 m_0 r_i \omega^2 \sin \omega t = F_y \sin \omega t \quad (1)$$

where,  $m_0$  is the eccentric mass,  $F_y$  is the excitation amplitude caused by unbalance mass,  $\omega$  is the excitation frequency.

### 2.2. SDOF nonlinear dynamic model of vehicle system

In this section, a SDOF lumped parameter dynamic model considering the nonlinear spring and nonlinear damper elements is presented to investigate the dynamic behaviors of vehicle system. The SDOF vehicle model is illustrated in Fig. 2, and the vehicle system is excited by a harmonic force  $F$ .

In Fig. 2,  $m$  represents the mass of the vehicle system. The suspension system is attached by means of nonlinear spring and damping, where  $f_k(y)$  and  $f_c(y, \dot{y})$  are the nonlinear spring force and damping force, respectively. Then, the forces can be written as follows:

$$\begin{aligned} f_k(y) &= k_1 y + k_2 y^2 + k_3 y^3, \\ f_c(y, \dot{y}) &= c_1 \frac{dy}{dt} + c_2 y \frac{dy}{dt} + c_3 y^2 \frac{dy}{dt}, \end{aligned} \quad (2)$$

where  $k_1$  and  $c_1$  represent the linear stiffness and damping,  $k_i$  and  $c_i$  ( $i=2, 3$ ) are the nonlinear stiffness and damping coefficients of the suspension.

According to the analysis of the nonlinear vehicle model, taking into the external excitation, the nonlinear spring force and damping force, and applying the Newton's second law of motion to the model in Fig. 2, the differential equation of the vibration system can be written as:

$$m \frac{d^2y}{dt^2} + f_k(y) + f_c(y, \dot{y}) = F - mg \quad (3)$$

Submitting the Eqs. (1) and (2) into Eq. (3), the equation of

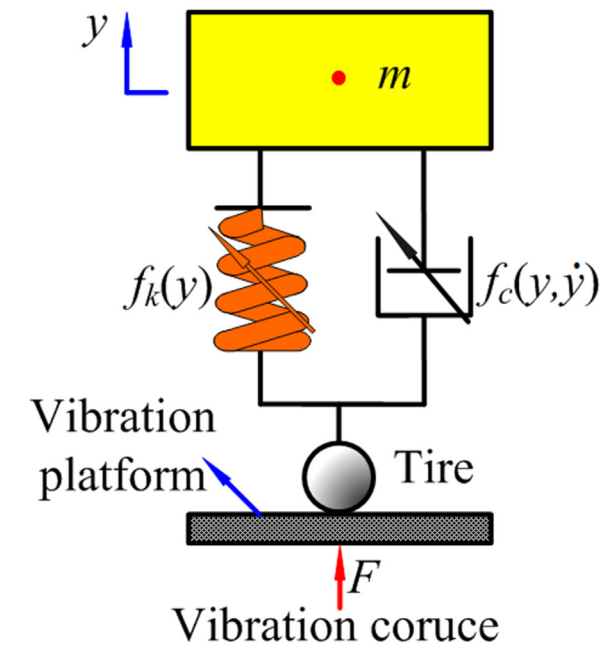


Fig. 2. Dynamic model of vehicle system.

motion can be rewritten as:

$$\begin{aligned} m \frac{d^2y}{dt^2} + \left( c_1 \frac{dy}{dt} + c_2 y \frac{dy}{dt} + c_3 y^2 \frac{dy}{dt} \right) + \left( k_1 y + k_2 y^2 + k_3 y^3 \right) \\ = F_y \sin \omega t - mg \end{aligned} \quad (4)$$

In engineering practice, the excitation frequency plays a dominant role in almost all cases. For analytical convenience, Eq. (4) can be dimensionless by using a characteristic length  $b$  and a characteristic frequency  $\omega_0$ . And the non-dimensional parameters can be expressed as follows:

$$x_i = \frac{y_i}{b}, \quad \tau = \omega_0 t, \quad \Omega = \frac{\omega}{\omega_0}, \quad \zeta = \frac{c_1}{m \omega_0}, \quad F_m = \frac{F_y}{mb \omega_0^2}. \quad (5)$$

Substituting Eq. (5) into Eq. (4), the dimensionless equation of motion of the system can be rewritten as:

$$\begin{aligned} \ddot{x} + \frac{c_1}{m \omega_0} \dot{x} + \frac{k_1}{m \omega_0^2} x = & - \frac{g}{b \omega_0^2} + \frac{F_y \sin(\Omega \tau)}{m b \omega_0^2} \\ & - \left( \frac{c_2 b}{m \omega_0} x \dot{x} + \frac{c_3 b^2}{m \omega_0} x^2 \dot{x} \right) \\ & - \left( \frac{k_2 b}{m \omega_0^2} x^2 + \frac{k_3 b^2}{m \omega_0^2} x^3 \right). \end{aligned} \quad (6)$$

In this study, Eq. (6) describes a SDOF vehicle nonlinear system. The approximate solution of the nonlinear differential equation is obtained using the IHBM and NMM. The equation can be represented in a matrix-vector form, which can be written as:

$$\mathbf{M}\ddot{\mathbf{X}} + \mathbf{C}\dot{\mathbf{X}} + \mathbf{K}\mathbf{X} = \mathbf{F}_L + \mathbf{F}_N \quad (7)$$

where,  $\mathbf{M}$ ,  $\mathbf{C}$  and  $\mathbf{K}$  are the mass matrix, damping matrix and stiffness matrix, respectively.  $\mathbf{F}_L$  is the linear factor vector, and  $\mathbf{F}_N$  is the nonlinear factor vector. It should be noted that the nonlinear force vector  $\mathbf{F}_N$  is a function of the displacement vector  $\mathbf{X}$  and the velocity vector  $\dot{\mathbf{X}}$ . The linear factor vector  $\mathbf{F}_L$  includes the external excitation and gravity.

$$\mathbf{M} = [1], \quad \mathbf{C} = \left[ \frac{c_1}{m\omega_0} \right], \quad \mathbf{K} = \left[ \frac{k_1}{m\omega_0^2} \right], \quad \mathbf{F}_L = \left[ \frac{-g}{b\omega_0^2} + \frac{F_y \sin \Omega\tau}{mb\omega_0^2} \right],$$

$$\mathbf{F}_N = \left[ -\left( \frac{c_2 b}{m\omega_0} x\dot{x} + \frac{c_3 b^2}{m\omega_0} x^2 \dot{x} \right) - \left( \frac{k_2 b}{m\omega_0^2} x^2 + \frac{k_3 b^2}{m\omega_0^2} x^3 \right) \right]$$

The simplified SDOF nonlinear model is able to verify the vibration characteristics, and presents the path transforms among the chaotic behavior, quasi-periodic motion and periodic (periodic- $n$ ) motion of the vehicle system. In addition, it can also approximate the dynamic response sufficiently to enable the results on the simple dynamic model to provide insight into the dynamics of the real vehicle with the external excitation.

### 3. Incremental harmonic balance method for nonlinear system

Consider the set of differential equations representing the nonlinear dynamic system of the following general form:

$$\mathbf{M}\ddot{\mathbf{X}} + \mathbf{C}\dot{\mathbf{X}} + \mathbf{K}\mathbf{X} + \mathbf{f}(\dot{\mathbf{X}}, \mathbf{X}) = \mathbf{P}(t) \quad (8)$$

where,  $\mathbf{M}$ ,  $\mathbf{C}$  and  $\mathbf{K}$  are mass, damping and stiffness matrices of vibration system, respectively.  $\mathbf{f}(\dot{\mathbf{X}}, \mathbf{X})$  is a nonlinear force function,  $\mathbf{X} = [x_1, x_2, \dots, x_i]^T$  is the degrees of freedom vector of the nonlinear system,  $i$  represents the number of the degrees of freedom,  $\mathbf{P} = [p_1, p_2, \dots, p_i]^T$  is the external harmonic excitation of the vehicle system.

In this paper, efforts are devoted to the application of the IHBM to a multi-degree of freedom (MDOF) nonlinear vehicle vibration system. So  $\tau = \omega t$ , and the Eq. (8) can be written as follows:

$$\omega^2 \mathbf{M}\ddot{\mathbf{X}} + \omega_0 \mathbf{C}\dot{\mathbf{X}} + \mathbf{K}\mathbf{X} + \mathbf{f}(\dot{\mathbf{X}}, \mathbf{X}) = \mathbf{P}(\tau) \quad (9)$$

where,  $\omega$  is excitation frequency of relevance; the dots denote derivatives with respect to dimensionless time  $\tau$ .

Using the Newton-Raphson procedure of the IHBM. Letting  $x_{i0}$ ,  $\omega$  denote a state of vibration in hand, the neighboring state can be expressed by adding the corresponding increments to them as follows:

$$\mathbf{X} = \mathbf{X}_0 + \Delta\mathbf{X}, \quad \omega = \omega_0 + \Delta\omega \quad (10)$$

here,  $\mathbf{X}_0 = [x_{10}, x_{20}, \dots, x_{i0}]^T$ ,  $\Delta\mathbf{X} = [\Delta x_1, \Delta x_2, \dots, \Delta x_i]^T$ .

In order to obtain periodic solutions to Eq. (9), a periodic solution can be obtained by expanding  $\mathbf{x}_i$ ,  $\mathbf{x}_{i0}$  and  $\Delta\mathbf{x}_i$  in a truncated finite Fourier series and applying the Galerkin's procedure. The periodic response can be expressed as follows:

$$x_i(\tau) = a_{i0} + \sum_{n=1}^N (a_{in} \cos(n\tau) + b_{in} \sin(n\tau)) = \mathbf{C}_s \mathbf{A}_i,$$

$$x_{i0}(\tau) = a_{i00} + \sum_{n=1}^N (a_{in0} \cos(n\tau) + b_{in0} \sin(n\tau)) = \mathbf{C}_s \mathbf{A}_{i0},$$

$$\Delta x_i(\tau) = \Delta a_{i0} + \sum_{n=1}^N (\Delta a_{in} \cos(n\tau) + \Delta b_{in} \sin(n\tau)) = \mathbf{C}_s \Delta \mathbf{A}_i, \quad (11)$$

where:  $N$  is the number of harmonics considered in the solution.

$$\mathbf{C}_s = \begin{bmatrix} 1 & \cos \tau & \sin \tau & \dots & \cos N\tau & \sin N\tau \end{bmatrix},$$

$$\mathbf{A}_i = \begin{bmatrix} a_{i0} & a_{i1} & b_{i1} & \dots & a_{iN} & b_{iN} \end{bmatrix}^T \mathbf{A}_{i0}$$

$$= \begin{bmatrix} a_{i00} & a_{i10} & b_{i10} & \dots & a_{iN0} & b_{iN0} \end{bmatrix}^T,$$

$$\Delta \mathbf{A}_i = \begin{bmatrix} \Delta a_{i0} & \Delta a_{i1} & \Delta b_{i1} & \dots & \Delta a_{iN} & \Delta b_{iN} \end{bmatrix}^T$$

Substituting Eq. (11) into Eq. (10), the vector of the vibration system can be expressed as follows:

$$\mathbf{X} = \mathbf{S}\mathbf{A}_i, \quad \mathbf{X}_0 = \mathbf{S}\mathbf{A}_{i0}, \quad \Delta\mathbf{X} = \mathbf{S}\Delta\mathbf{A} \quad (12)$$

where,

$$\mathbf{A} = [\mathbf{A}_1^T \quad \mathbf{A}_2^T \quad \dots \quad \mathbf{A}_i^T \quad \dots \quad \mathbf{A}_N^T]^T, \quad \mathbf{A}_0 = [\mathbf{A}_{10}^T \quad \mathbf{A}_{20}^T \quad \dots \quad \mathbf{A}_{i0}^T \quad \dots \quad \mathbf{A}_{N0}^T]^T$$

$$\Delta\mathbf{A} = [\Delta\mathbf{A}_1^T \quad \Delta\mathbf{A}_2^T \quad \dots \quad \Delta\mathbf{A}_i^T \quad \dots \quad \Delta\mathbf{A}_N^T]^T, \quad \mathbf{S} = \text{diag}[\mathbf{C}_s \quad \mathbf{C}_s \quad \dots \quad \mathbf{C}_s]_{N \times iN}$$

Substituting Eq. (12) into Eq. (9) and neglecting small terms of high order, it can obtain the following equation:

$$\omega_0^2 \mathbf{M}\ddot{\mathbf{X}} + \omega_0 \mathbf{C}\dot{\mathbf{X}} + \mathbf{K}\mathbf{X} + \mathbf{C}_n \Delta\dot{\mathbf{X}} + \mathbf{K}_n \Delta\mathbf{X}$$

$$= \mathbf{P}(\tau) - \mathbf{f}_n(\mathbf{X}_0, \dot{\mathbf{X}}_0) - (\omega_0^2 \mathbf{M}\ddot{\mathbf{X}}_0 + \omega_0 \mathbf{C}\dot{\mathbf{X}}_0 + \mathbf{K}\mathbf{X}_0)$$

$$- (2\omega_0 \mathbf{M}\ddot{\mathbf{X}}_0 + \mathbf{C}\dot{\mathbf{X}}_0) \Delta\omega \quad (13)$$

where,  $\mathbf{C}_n = \frac{\partial \mathbf{f}_n(\mathbf{X}, \dot{\mathbf{X}})}{\partial \mathbf{X}}$ ,  $\mathbf{K}_n = \frac{\partial \mathbf{f}_n(\mathbf{X}, \dot{\mathbf{X}})}{\partial \dot{\mathbf{X}}}$ ,  $\mathbf{C}_n$  and  $\mathbf{K}_n$  are the Jacobian matrixes.

Assumption  $\delta\mathbf{x} = \mathbf{S}\delta\mathbf{A}$ , and using the Galerkin procedure gives:

$$\int_0^{2\pi} \delta(\mathbf{X})^T [\omega_0^2 \mathbf{M}\ddot{\mathbf{X}} + \omega_0 \mathbf{C}\dot{\mathbf{X}} + \mathbf{K}\mathbf{X} + \mathbf{C}_n \Delta\dot{\mathbf{X}} + \mathbf{K}_n \Delta\mathbf{X}] d\tau$$

$$= \int_0^{2\pi} \delta(\mathbf{X})^T [\mathbf{P}(\tau) - \mathbf{f}_n(\mathbf{X}_0, \dot{\mathbf{X}}_0) - (\omega_0^2 \mathbf{M}\ddot{\mathbf{X}}_0 + \omega_0 \mathbf{C}\dot{\mathbf{X}}_0 + \mathbf{K}\mathbf{X}_0)$$

$$- (2\omega_0 \mathbf{M}\ddot{\mathbf{X}}_0 + \mathbf{C}\dot{\mathbf{X}}_0) \Delta\omega] d\tau. \quad (14)$$

Substituting Eq. (12) into Eq. (14) and simplified by:

$$\int_0^{2\pi} (\delta\mathbf{A})^T \mathbf{S}^T [\omega_0^2 \mathbf{M}\ddot{\mathbf{X}} + \omega_0 \mathbf{C}\dot{\mathbf{X}} + \mathbf{K}\mathbf{X} + \mathbf{C}_n \Delta\dot{\mathbf{X}} + \mathbf{K}_n \Delta\mathbf{X}] d\tau$$

$$= \int_0^{2\pi} (\delta\mathbf{A})^T \mathbf{S}^T [\mathbf{P}(\tau) - \mathbf{f}_n(\mathbf{X}_0, \dot{\mathbf{X}}_0) - (\omega_0^2 \mathbf{M}\ddot{\mathbf{X}}_0 + \omega_0 \mathbf{C}\dot{\mathbf{X}}_0 + \mathbf{K}\mathbf{X}_0)$$

$$- (\omega_0^2 \mathbf{M}\ddot{\mathbf{X}}_0 + \omega_0 \mathbf{C}\dot{\mathbf{X}}_0 + \mathbf{K}\mathbf{X}_0) \Delta\omega] d\tau. \quad (15)$$

According to the variational characteristics, the Eq. (15) can be expressed as follow:

$$\int_0^{2\pi} \mathbf{S}^T [\omega_0^2 \mathbf{M}\ddot{\mathbf{X}} + \omega_0 \mathbf{C}\dot{\mathbf{X}} + \mathbf{K}\mathbf{X} + \mathbf{C}_n \Delta\dot{\mathbf{X}} + \mathbf{K}_n \Delta\mathbf{X}] d\tau \cdot \Delta\mathbf{A}$$

$$= - \int_0^{2\pi} \mathbf{S}^T (\omega_0^2 \mathbf{M}\ddot{\mathbf{X}} + \omega_0 \mathbf{C}\dot{\mathbf{X}} + \mathbf{K}\mathbf{X}) d\tau \cdot \mathbf{A}_0$$

$$+ \int_0^{2\pi} \mathbf{S}^T [\mathbf{P}(\tau) - \mathbf{f}_n(\mathbf{X}_0, \dot{\mathbf{X}}_0)] d\tau$$

$$- \int_0^{2\pi} \mathbf{S}^T (2\omega_0 \mathbf{M}\ddot{\mathbf{X}}_0 + \mathbf{C}\dot{\mathbf{X}}_0) d\tau \cdot \mathbf{A}_0 \Delta\omega. \quad (16)$$

Therefore, a set linear equations in terms of  $\Delta\mathbf{A}$  and  $\Delta\omega$  can be obtained readily:

$$\mathbf{K}_m \Delta\mathbf{A} = \mathbf{R}_{m1} \mathbf{A}_0 + \mathbf{R}_{m2} + \mathbf{R}_{m3} \mathbf{A}_0 \Delta\omega \quad (17)$$

where,

**Table 1**  
Main parameters for the vehicle system.

Parameter	Value
$m_1$	unsprung mass (kg)
$g$	gravitational acceleration (m/s <sup>2</sup> )
$k_1/k_2/k_3$	sprung mass spring coefficient (N/m)/(N/m <sup>2</sup> )/(N/m <sup>3</sup> )
$c_1/c_2/c_3$	sprung mass damping coefficient (Ns/m)/(Ns/m <sup>2</sup> )/(Ns/m <sup>3</sup> )

$$\begin{aligned} \mathbf{K}_m &= \int_0^{2\pi} \mathbf{S}^T [\omega_0^2 \mathbf{M} \ddot{\mathbf{S}} + \omega_0 \mathbf{C} \dot{\mathbf{S}} + \mathbf{K} \mathbf{S} + \mathbf{C}_n \dot{\mathbf{S}} + \mathbf{K}_n \mathbf{S}] d\tau, \\ \mathbf{R}_{m1} &= - \int_0^{2\pi} \mathbf{S}^T (\omega_0^2 \mathbf{M} \ddot{\mathbf{S}} + \omega_0 \mathbf{C} \dot{\mathbf{S}} + \mathbf{K} \mathbf{S}) d\tau, \\ \mathbf{R}_{m2} &= \int_0^{2\pi} \mathbf{S}^T [\mathbf{P}(\tau) - \mathbf{f}_n(\mathbf{X}_0, \dot{\mathbf{X}}_0)] d\tau, \\ \mathbf{R}_{m3} &= - \int_0^{2\pi} \mathbf{S}^T (2\omega_0 \mathbf{M} \ddot{\mathbf{S}} + \mathbf{C} \dot{\mathbf{S}}) d\tau. \end{aligned} \quad (18)$$

#### 4. Investigation of parameter influence on dynamic characteristics

From the previous conclusions and analysis, it can be seen that the vehicle model is a complicated system with the strong nonlinearity, time variance and complicated running conditions. Therefore, it is necessary to give a detailed analysis of the vehicle vibration system. The equation of motion described by Eq. (6) for the vehicle system with nonlinear stiffness and damping effects is simulated by the IHBM and NMM. On this basis, some key parameters of the vehicle system are selected to study the dynamic behaviors, and the system geometry parameters are given in Table 1. The chaotic behavior of the vehicle nonlinear system should be suppressed reasonably due it will aggravate the destructiveness and insecurity of the vehicle system. Therefore, it is necessary to analyze the parameter adjustment of the external excitation for inhibiting the chaotic vibration effectively. In this section, a series of simulations are carried out. The purpose is to examine the influences of the damping coefficient  $\zeta$  ( $\zeta = c_1/m\omega_0$ ), excitation amplitude  $F_m$  ( $F_m = F_y/mb\omega_0^2$ ) and excitation frequency  $\Omega$  ( $\Omega = \omega/\omega_0$ ) on the dynamic responses. In order to better understand the dynamic responses of the system intuitively, the detailed simulation condition schematic is shown in Fig. 3.

#### 4.1. The validation of analytical method

In order to demonstrate the effectiveness and accuracy of the IHBM, the nonlinear dynamic responses of the SDOF vehicle system are obtained by adopting the IHBM and NMM. The predicted dynamic responses are plotted in Fig. 4 and Fig. 5, and the responses match with each other well. Here, Fig. 4 shows the comparison of the vibration displacement and phase diagrams at  $\Omega=0.5$  Figs. 4(a) and (b) and  $\Omega=1.0$  Fig. 4(c) and (d) of the vibration system. In Fig. 4, the blue solid line denotes the numerical results by the NMM and the red circle represents the steady state calculation results by the IHBM, respectively. It can be seen that the vehicle system has strong nonlinear characteristics, and the nonlinear dynamic responses under the external harmonic excitation is not constituted by the linear superposition.

In order to analyze the nonlinear dynamic characteristics of the SDOF vehicle system, the amplitude-frequency curves are shown in Fig. 5, where the horizontal axis is the excitation frequency  $\Omega$ , and the vertical axis indicates the maximum  $x_{max}$  or minimum  $x_{min}$  of nonlinear vibration displacements. It is indicated that the results by IHBM agree with the NMM's, which verifies the precision of the IHBM presented in this paper to have high enough. In addition, it takes 500 cycles and 139s, when the vehicle nonlinear system closes to steady state response of convergence by NMM. However, the IHBM only needs 31s, it can be observed that the accuracy by IHBM presented in this paper is reliable with the NMM. In Fig. 5, the nonlinear characteristics of multi-valued property, super-harmonic frequency and hardening/softening type nonlinear behaviors appear in the amplitude-frequency curves (Table 2).

Fig. 6 shows the amplitude-frequency curves of  $x_{max}$  and  $x_{min}$  for different harmonic number for  $N=1$ ,  $N=8$  and  $N=15$ . It can be observed from Fig. 6 that the amplitude-frequency curves appear different variation tendency. Only the primary resonance exists at  $N=1$ , and it is accurate overall frequency spans without any sign of a super-harmonic dimple as found. When  $N=8$ , the primary resonance increases markedly and the slope slightly increases (in the

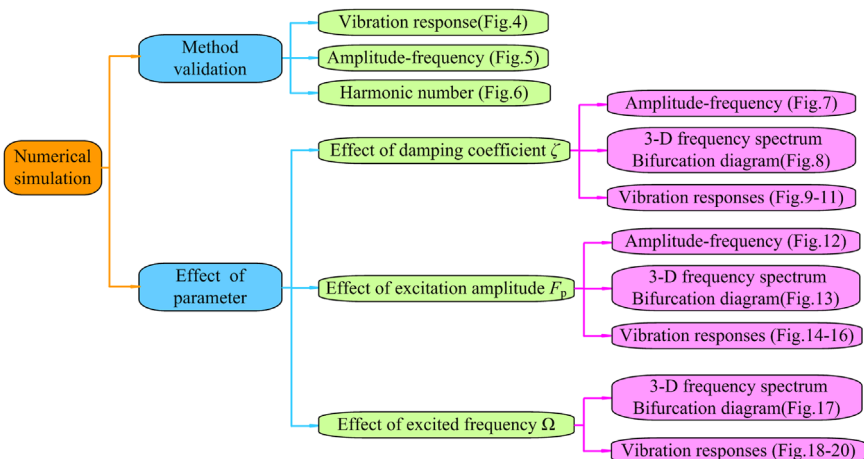
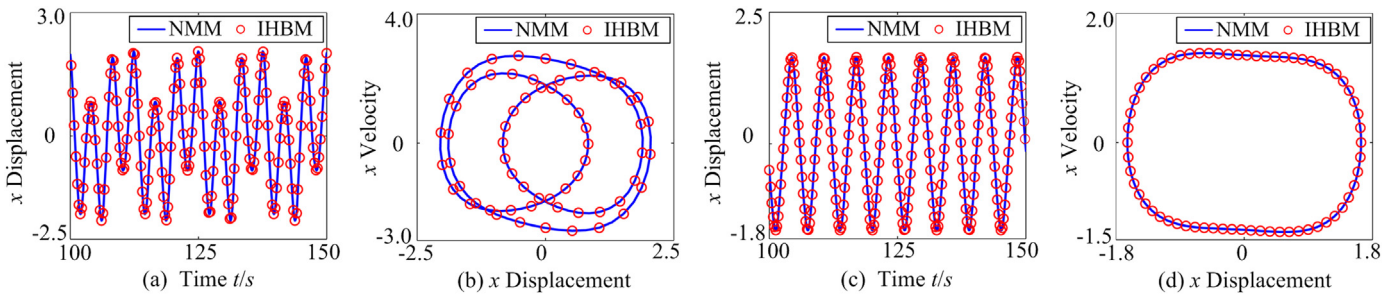


Fig. 3. Simulation condition schematic.



**Fig. 4.** Vibration waveforms and phase diagrams of the vehicle system at  $\Omega=0.5$  and  $\Omega=1.0$ . (For interpretation of the references to color in this figure, the reader is referred to the web version of this article.).

regimes “B” and “D”). Particularly, the super-harmonic resonance peaks exhibit in locations “A” and “C”. However, compared with  $N=8$ , the amplitude-frequency curve has almost no change at  $N=15$ . Furthermore, the quasi-periodic motion or chaotic motion is possible appearance in “A” and “C”. It is noted from Fig. 6 that the harmonic number  $N$  should be selected the appropriate value, which has a certain effect on the nonlinearity. When  $N$  is small ( $N=1$ ), the super-harmonic resonances can't be observed and reduces the calculation accuracy. Conversely, with the increasing of  $N$ , the calculation accuracy is improved but the computation time will increase. Therefore, under the comprehensive consideration, the harmonic number is selected  $N=8$  in this paper.

In the following sections, a series of parametric studies are carried out. The purpose is to investigate the influences of the dynamic characteristics with the damping coefficient  $\zeta$ , excitation amplitude  $F_m$  and excitation frequency  $\Omega$ .

#### 4.2. Effect of the damping coefficient $\zeta$ on dynamic response of system

In order to investigate the effect of the damping coefficient  $\zeta$  on the vibration characteristics, the amplitude-frequency curves are shown in Fig. 7 with four groups of damping coefficients  $\zeta=0.005$ ,  $\zeta=0.05$ ,  $\zeta=0.08$  and  $\zeta=0.1$ . With the increasing damping coefficient  $\zeta$ , the variation tendency of the amplitude-frequency curves of  $x_{max}$  and  $x_{min}$  remain the same, but the overall amplitudes increase and the region of multi-valued properties in the amplitude-frequency responses of the system narrow down ( $\zeta=0.005$ ,  $\Omega \in [1.56, 2.78]$ ;  $\zeta=0.05$ ,  $\Omega \in [1.54, 1.78]$ ;  $\zeta=0.08$ ,  $\Omega \in [1.55, 2.42]$ ;  $\zeta=0.1$ ,  $\Omega \in [1.52, 1.59]$ ). In addition, the damping coefficient  $\zeta$  makes the system present a hardening type nonlinear behavior. For low value  $\Omega < 0.24$ , the increasing  $\zeta$  has little or no effect on the amplitude. When  $\Omega$  increases from 0.24 to 2.1, the increasing

**Table 2**

Comparison between IHBM and NMM for the system of Fig. 4(c).

	IHBM	NMM
Amplitude ( $x$ )	4.18	4.19
Computation time ( $t$ )	31s	139s

damping coefficient  $\zeta$  makes the amplitude evident decrease. Particularly, spur-harmonic peaks ( $\omega/2$ ,  $2\omega/3$ ) exhibit, and the unstable solution region associated with the spur-harmonic response diminishes slightly with increasing  $\zeta$ . When  $\Omega > 2.1$ , the damping coefficient  $\zeta$  has little influence on the vibration amplitude. It can be observed that the damping coefficient  $\zeta$  has less effect on the nonlinear dynamic properties at lower ( $\Omega < 0.24$ ) and higher ( $\Omega > 2.1$ ) values.

Fig. 8 indicates the effects of the damping coefficient on the 3-D frequency spectrum and bifurcation diagram with  $\zeta$  as the control parameter. It can be observed that the system exhibits strong nonlinear characteristics with the effect of damping coefficient  $\zeta$ . When the damping coefficient increases from  $0.5 \times 10^{-2}$  to  $5.2 \times 10^{-2}$ , the 3-D frequency spectrum of the SDOF system includes demultiplication frequency ( $0.5f$ ) and multiplication frequency ( $f, 2f, 5f, 8f, 9f$ ) components. The amplitude of  $f$  is the grater than others in the range of  $[0.5, 1.9] \times 10^{-2}$ , and the amplitude of multiplication frequency ( $3f$ ) is the dominated response at  $\zeta > 1.9 \times 10^{-2}$  and the amplitude increases markedly. Due to the low damping coefficient, the system presents chaotic motion. With the increase of damping coefficient, the continuous frequency components fade away gradually, and the  $3f$  is the dominated in 3-D frequency spectrum. Moreover, other frequency amplitudes reduce slightly. Combined with the corresponding bifurcation diagram, the chaotic motion transits to periodic-2 motion. As further increase from  $6.8 \times 10^{-2}$  to  $10 \times 10^{-2}$ , the system enters

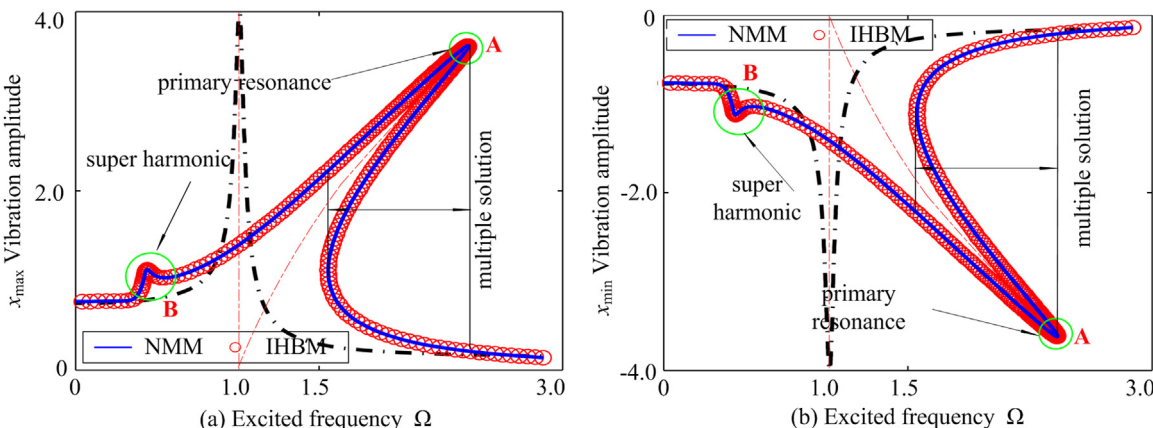


**Fig. 5.** Comparison between IHBM and NMM. — NMM, ○ IHBM. (For interpretation of the references to color in this figure, the reader is referred to the web version of this article.).

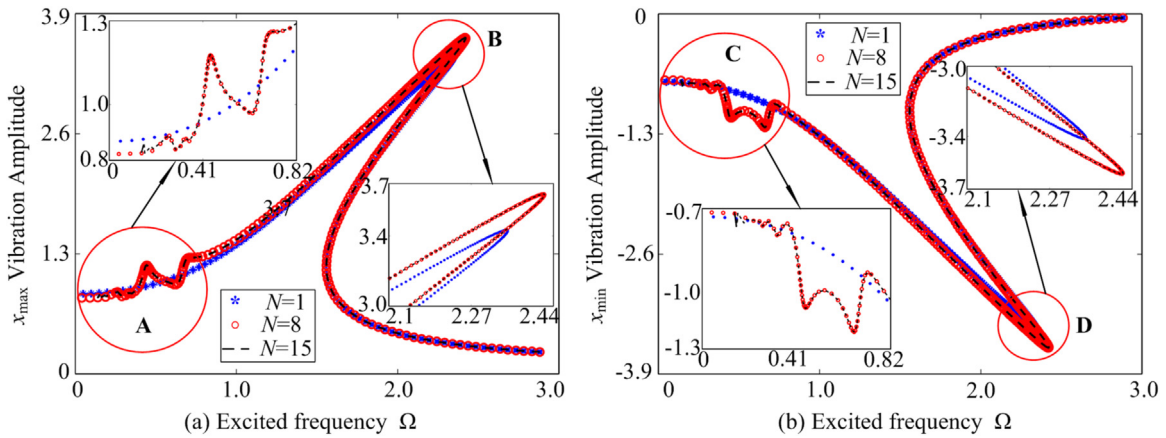


**Fig. 6.** Amplitude-frequency curves of  $x_{max}$  and  $x_{min}$  for  $N$ . \*  $N=1$ , o  $N=8$ , –  $N=15$ . (For interpretation of the references to color in this figure, the reader is referred to the web version of this article.).

into periodic-1 motion, and the vibration intensity weakens.

In order to investigate more deeply, the vibration responses of the SDOF vehicle system under  $\zeta=0.007$ ,  $\zeta=0.06$ ,  $\zeta=0.1$  are shown in Figs. 9–11. It can be observed from figures that the system exists the transferring process from chaotic behavior to periodic motion with the increasing  $\zeta$ . It can be concluded from the response diagrams that an increase of the damping coefficient  $\zeta$  can cause an obvious decrease the vibration amplitude.

#### 4.3. Effect of the excitation amplitude $F_m$ on dynamic response of system

In this section, the effect of the excitation amplitude  $F_m$  on the dynamic responses are investigated by IHBM, and the other parameters remain the same. The amplitude-frequency curves for four different excitation amplitudes ( $F_m=0.1$ ,  $F_m=0.5$ ,  $F_m=1.0$ ,  $F_m=1.5$ ) are analyzed and compared in Fig. 12. With the increasing excitation amplitude  $F_m$ , the primary resonance amplitudes increase markedly. However, it is noteworthy that the nonlinear dynamic characteristics such as multi-valued properties and hardening type nonlinear behavior gradually strengthened. From Fig. 12, the increasing excitation amplitude  $F_m$  makes the vibration amplitude increase obviously in the range of  $\Omega \in [0, 1.9]$ . While the effect of the vibration amplitude relatively diminishes at  $\Omega > 1.9$ . When the excitation amplitude is low ( $F_m=0.1$ ), the nonlinear characteristics of spur-harmonic resonance, hardening type behavior and multi-valued property ( $\Omega \in [1.16, 1.27]$ ) gradually

vanish, which cannot properly predict the spur-harmonic response and accurately reflect the dynamic characteristics of the vibration system. When the excitation amplitude increases heavily ( $F_m=0.5$ ,  $F_m=1.0$ ,  $F_m=1.5$ ), the spur-harmonic resonance regions have an obvious change  $\Omega \in [0.33, 0.65]$  at  $F_m=0.5$ ,  $\Omega \in [0.35, 0.76]$  at  $F_m=1.0$  and  $\Omega \in [0.44, 0.92]$  at  $F_m=1.5$ . In addition, the multi-valued regions also broaden distinctly  $\Omega \in [1.39, 1.94]$  at  $F_m=0.5$ ,  $\Omega \in [1.57, 2.42]$  at  $F_m=1.0$  and  $\Omega \in [1.90, 3.30]$  at  $F_m=1.5$ . Therefore, it can be observed that the increasing excitation amplitude expands the multi-valued region, increases the vibration amplitude and intensifies the vibration extension. The peak value of the primary resonance increases appreciably with the increasing excitation amplitude.

Fig. 13 shows the 3-D frequency spectrum and bifurcation diagram of the vibration system, where excitation amplitude  $F_m$  is treated as the control parameter from 0.3 to 4.0. It is clear that the  $f$  is the main frequency component in the range of [0.3, 1.43], and the amplitude of  $f$  increases slightly. The periodic-1 motion is shown in Fig. 13(b). With the increase of  $F_m$  from 1.43 to 1.90, the demultiplication frequency ( $7f/3$ ) and multiplication frequency ( $f$  and  $3f$ ) components appear, and the corresponding bifurcation diagram transforms to quasi-periodic motion. In addition, the amplitudes of  $f$  and  $7f/3$  increase slightly with the variational excitation amplitude  $F_m$ . When  $F_m$  increases from 1.90 to 2.35, the frequency components remain about the same, and the amplitudes fluctuates obviously. In Fig. 13(b), a path to periodic motion through quasi-periodic motion is observed, and the typical

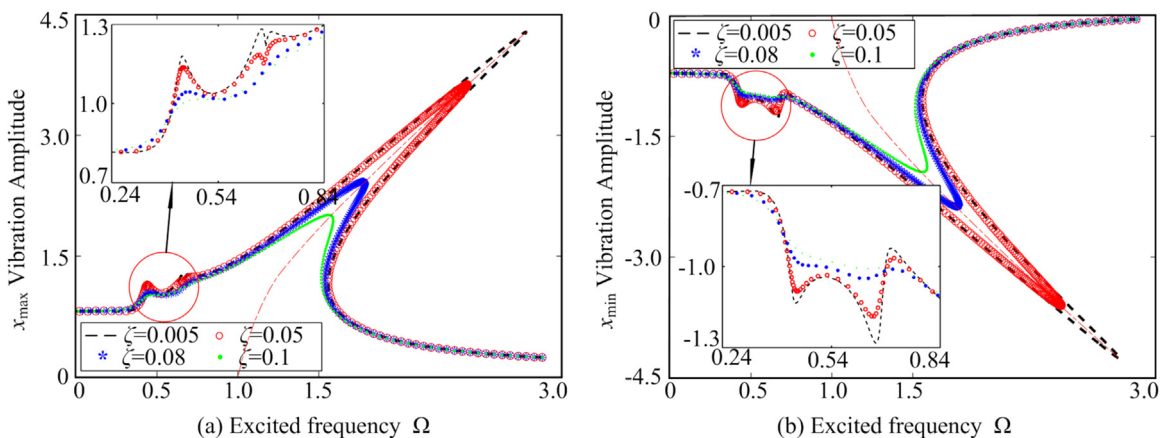


**Fig. 7.** Effect of damping coefficient on amplitude-frequency curves for  $\zeta$ . –  $\zeta=0.005$ , o  $\zeta=0.05$ , \*  $\zeta=0.08$ , •  $\zeta=0.1$ : (a)  $x_{max}$  (b)  $x_{min}$ . (For interpretation of the references to color in this figure, the reader is referred to the web version of this article.).

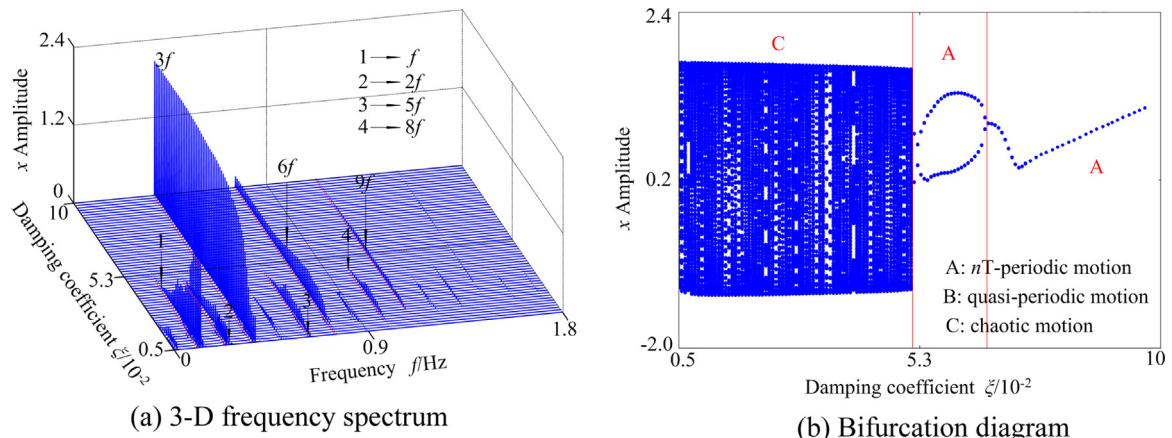


**Fig. 8.** 3-D frequency spectrum and bifurcation diagram using  $\zeta$  as control parameter. (a) 3-D frequency spectrum (b) Bifurcation diagram.

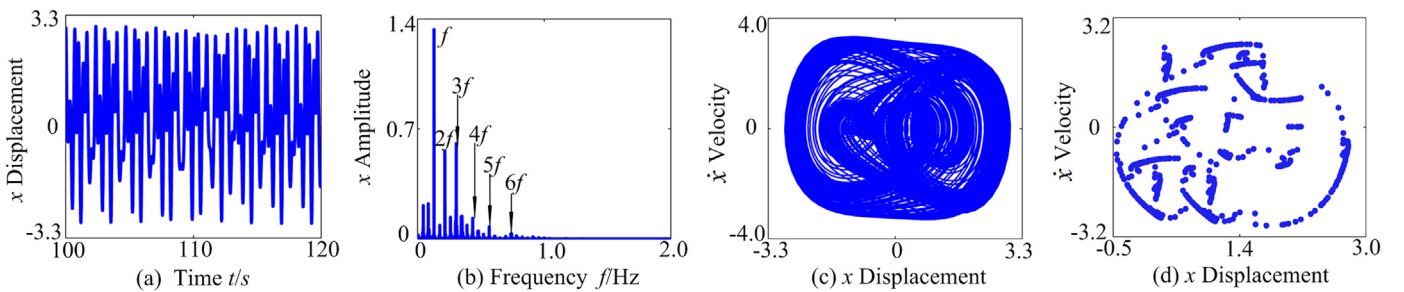


**Fig. 9.** Vibration response of the vehicle system at  $\zeta=0.007$ . (a) Waveform, (b) Frequency, (c) Phase diagram, and (d) Poincaré map.

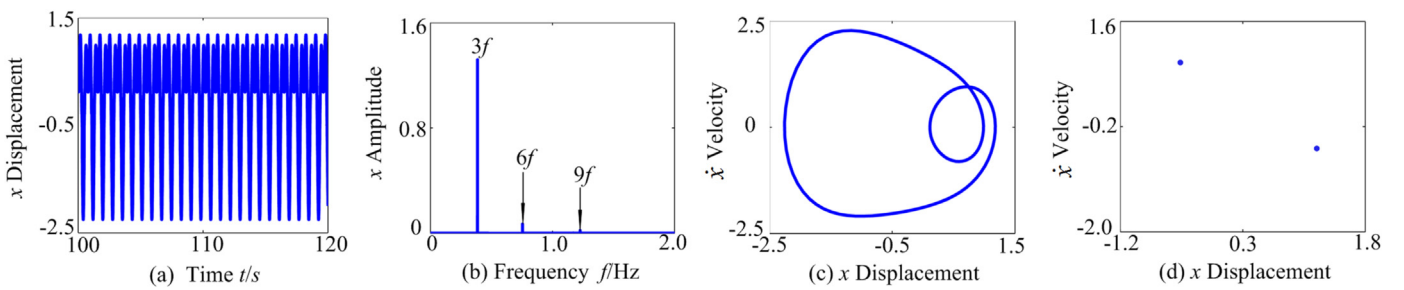


**Fig. 10.** Vibration response of the vehicle system at  $\zeta=0.06$ . (a) Waveform, (b) Frequency, (c) Phase diagram, and (d) Poincaré map.

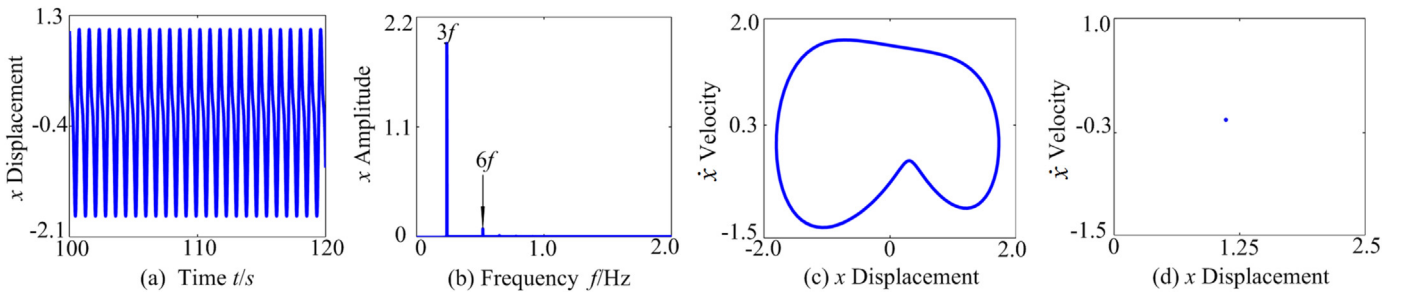


**Fig. 11.** Vibration response of the vehicle system at  $\zeta=0.1$ . (a) Waveform, (b) Frequency, (c) Phase diagram, and (d) Poincaré map.

nonlinear of jump discontinuity exists. The complicated frequency components about  $f/3$ ,  $f$ ,  $7f/3$ ,  $3f$ ,  $13f/3$ , continuous frequency, etc. exist, and the amplitudes increase obviously in the range of [2.35, 3.9], which indicates that the vibration is intensified. In bifurcation diagram, the system exhibits chaotic motion though periodic

motion. For  $F_m$  greater than 3.9, the continuous frequency components withdraw gradually and the  $f$  is the dominated response. The chaotic motion is replaced by periodic-3 motion.

The vibration responses under three excitation amplitudes  $F_m$  for  $F_m = 1.0$ ,  $F_m = 1.5$ ,  $F_m = 2.7$  are shown in Figs. 14–16. Compared

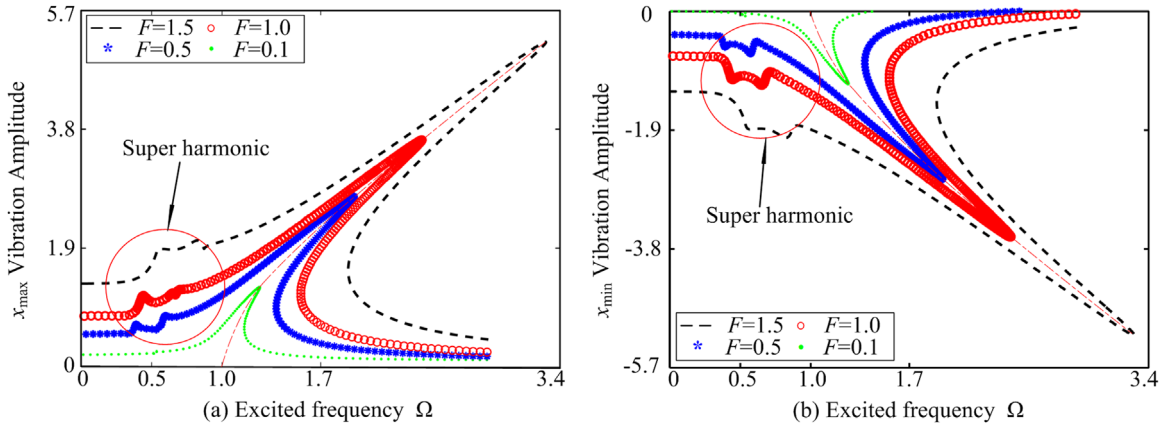


**Fig. 12.** Effect of excitation amplitude on amplitude-frequency curves for  $F_m$ . –  $F_m = 1.5$ , o  $F_m = 1.0$ , \*  $F_m = 0.5$ , •  $F_m = 0.1$ : (a)  $x_{\max}$  (b)  $x_{\min}$ .

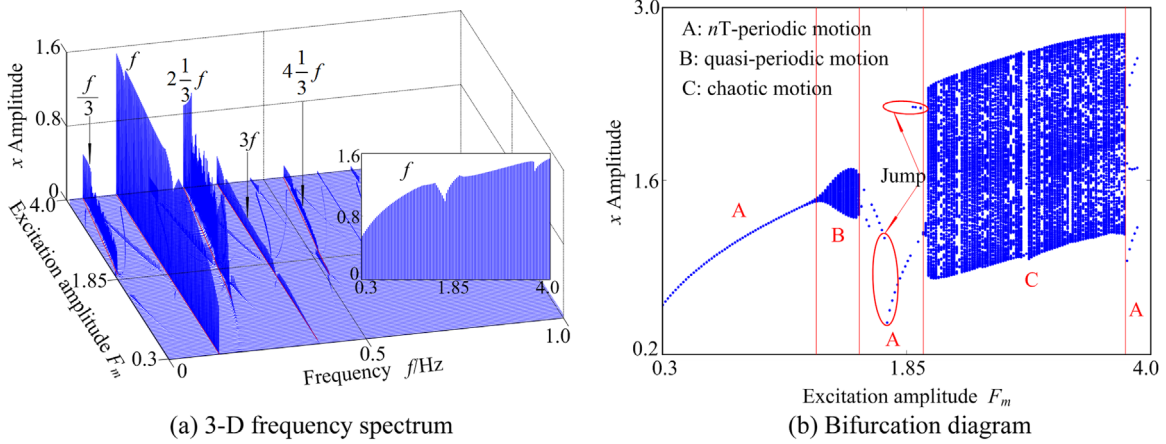


**Fig. 13.** 3-D frequency spectrum and bifurcation diagram using  $F_m$  as control parameter. (a) 3-D frequency spectrum, and (b) Bifurcation diagram.

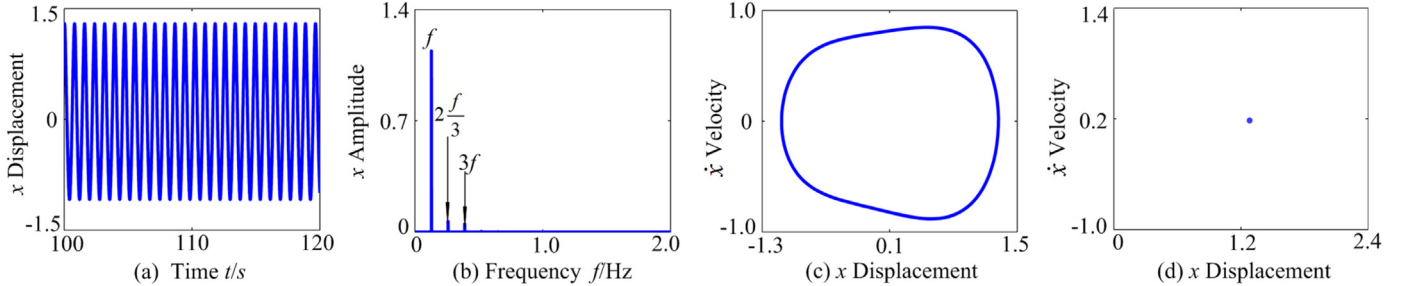


**Fig. 14.** Vibration response of the vehicle system at  $F_m = 1.0$ . (a) Waveform, (b) Frequency, (c) Phase diagram, and (d) Poincaré map.

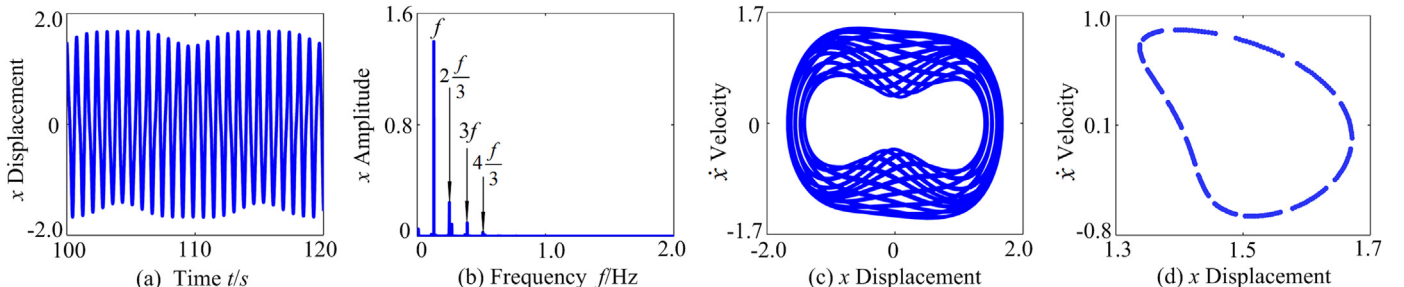


**Fig. 15.** Vibration response of the vehicle system at  $F_m = 1.5$ . (a) Waveform, (b) Frequency, (c) Phase diagram, and (d) Poincaré map.

with the figures, the vibration amplitude increases gradually, as shown in Figs. 14(a)–16(a). The  $f$  is the dominated response in Figs. 14(b)–16(b), and the frequency components significantly

change from discrete frequency components to continuous frequency components. The phase diagrams and Poincaré maps can be verified that the system exists periodic motion, quasi-periodic

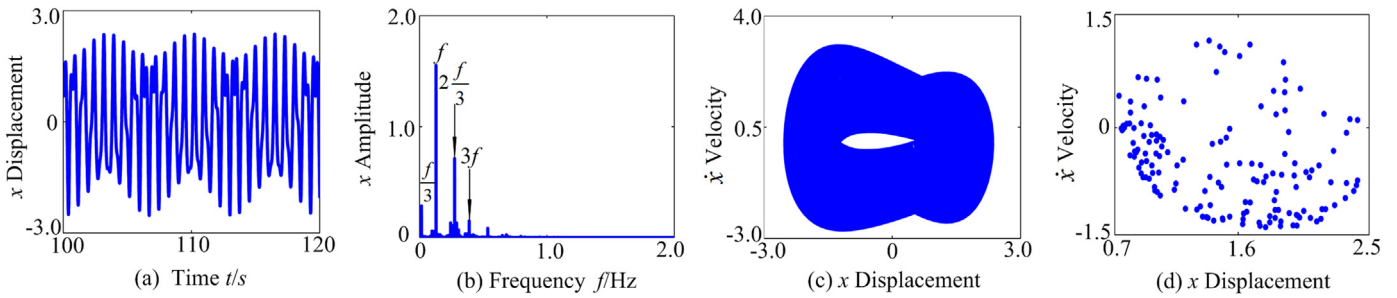


Fig. 16. Vibration response of the vehicle system at  $F_m=2.7$ . (a) Waveform, (b) Frequency, (c) Phase diagram, and (d) Poincaré map.

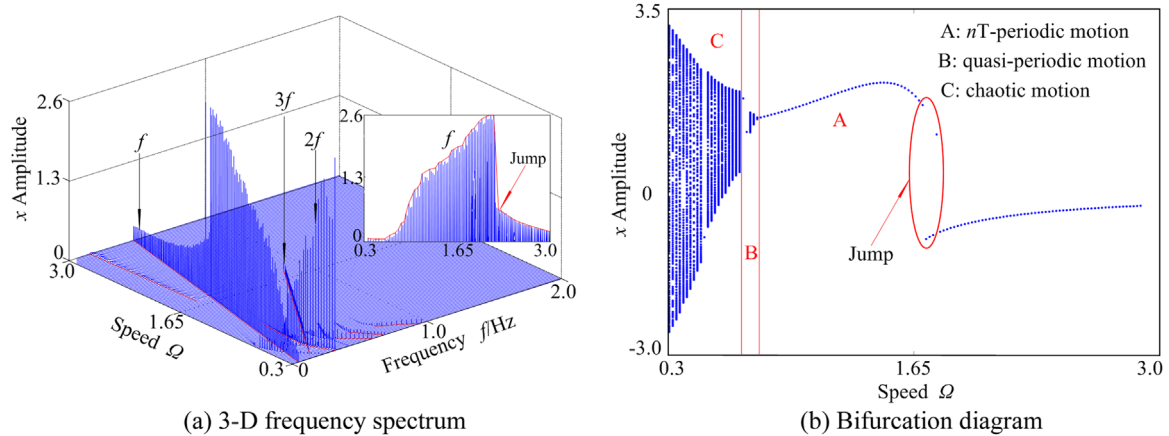


Fig. 17. 3-D frequency spectrum and bifurcation diagram using  $\Omega$  as control parameter. (a) 3-D frequency spectrum (b) Bifurcation diagram.

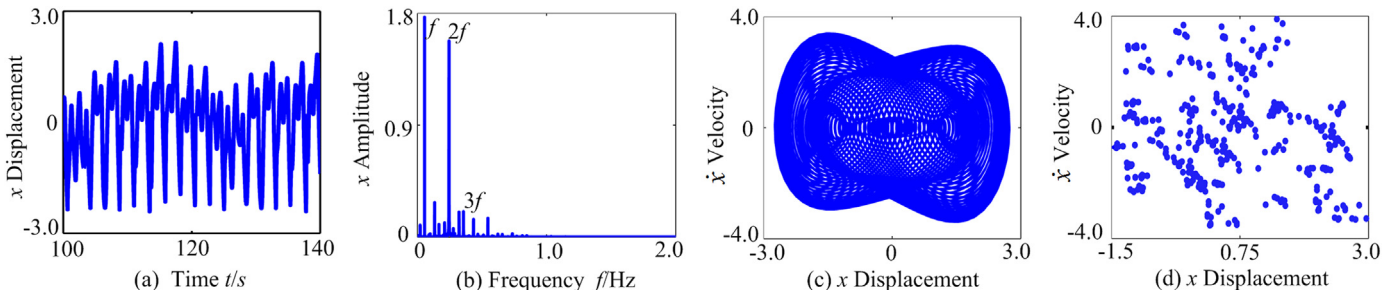


Fig. 18. Vibration response of the vehicle system at  $\Omega=0.4$ . (a) Waveform, (b) Frequency, (c) Phase diagram, and (d) Poincaré map.

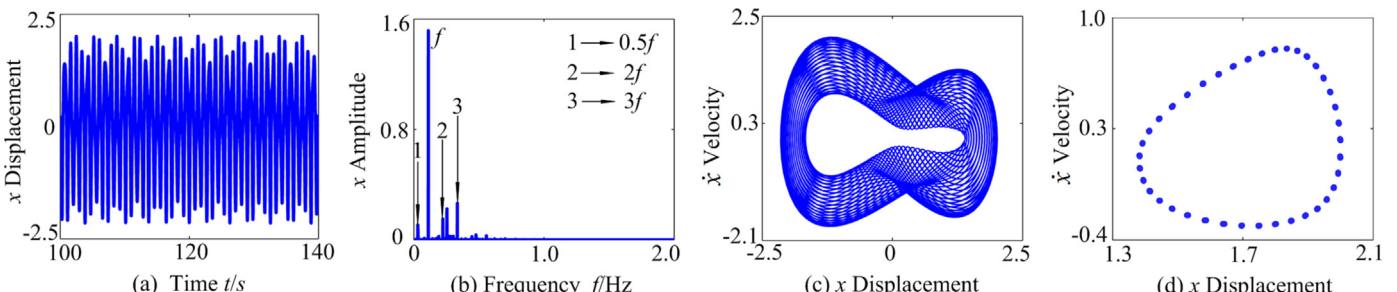


Fig. 19. Vibration response of the vehicle system at  $\Omega=0.75$ . (a) Waveform, (b) Frequency, (c) Phase diagram, and (d) Poincaré map.

motion and chaotic behavior.

#### 4.4. Effect of the excitation frequency $\Omega$ on dynamic response of system

Based on the above analysis, it is clear that the excitation frequency  $\Omega$  is an important parameter influencing the nonlinear characteristics. Fig. 17 illustrates the 3-D frequency spectrum and bifurcation diagram of the SDOF vehicle nonlinear vibration

system with  $\Omega$  as control parameter in the range of  $\Omega \in [0.3, 3.0]$ . It can be observed from Figs. 17 that the vehicle system presents complicated dynamic properties. The vibration system shows different periodic motion, quasi-periodic motion and chaotic motion. At low excitation frequency, i.e.  $0.3 < \Omega < 0.71$ , the 3-D frequency spectrum (Fig. 17(a)) of the vibration system in different rotational speed ranges includes complicated demultiplication frequency ( $0.5f$ ) and multiplication frequency ( $f$ ,  $2f$  and  $3f$ ) components. The amplitude of  $f$  increases gradually, and the amplitude of

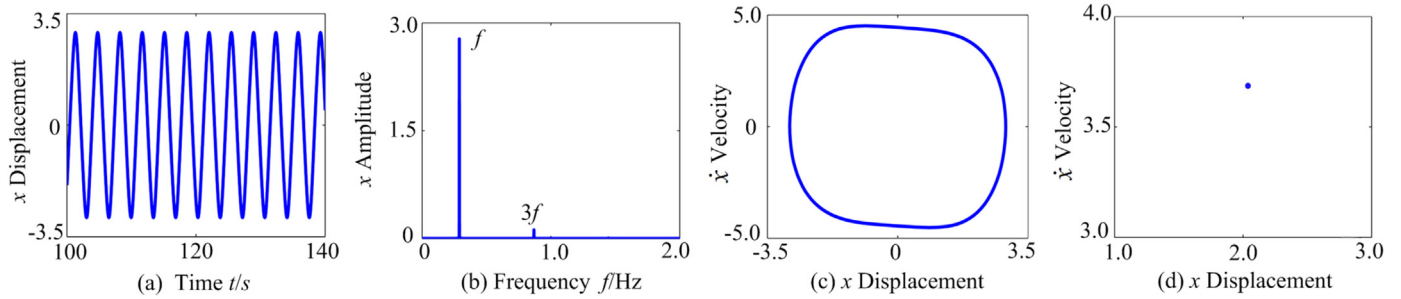


**Fig. 20.** Vibration response of the vehicle system at  $\Omega=1.8$ . (a) Waveform, (b) Frequency, (c) Phase diagram, and (d) Poincaré map.

multiplication frequency  $2f$  increases first and then decreases, which reaches the maximum value at  $\Omega=0.4$ . In addition, the  $2f$  is the dominated response. In corresponding to the bifurcation diagram, the system motion is from chaotic motion at  $0.3 < \Omega < 0.5$ , through periodic motion in the range of  $[0.5, 0.52]$ , to chaotic motion at  $0.52 < \Omega < 0.71$ . With the increase of excitation frequency  $\Omega$  from 0.71 to 0.83, the  $f$  is dominant and the amplitude of  $f$  is maximal, which increases sharply. Besides, the  $3f$  can be observed and the amplitude of  $3f$  increases slightly. In bifurcation diagram, a transient periodic motion at  $[0.71, 0.73]$  is replaced by quasi-periodic motion in the range of  $[0.73, 0.83]$ . Finally, when  $\Omega > 0.83$ , the demultiplication frequency  $0.5f$  and  $f$  appear. The amplitude of  $f$  increases markedly and decreases sharply compared with other frequency components, which reaches to the peak value at  $\Omega=0.83$ . The motion synchronous with periodic motion and only one point is correspondingly shown in bifurcation diagram and the jump discontinuity appears near  $\Omega=1.75$ .

The vibration waveforms, frequency spectrums, phase diagrams and Poincaré maps are shown in Figs. 18–20 for  $\Omega=0.4$ ,  $\Omega=0.75$  and  $\Omega=1.8$ . As shown in Fig. 18, the SDOF system presents chaotic motion, which can be reflected by a periodic vibration waveform, continuous frequency and irregular phase diagram and Poincaré map. When  $\Omega=0.75$ , it is clearly observed that the system is quasi-periodic motion due to the appearance of a close circle, and some frequency components have no common divisor. Fig. 20 shows the vibration of the system at  $\Omega=1.8$ . It can be found that the system enters to periodic-1 motion from quasi-periodic motion and only one point is correspondingly shown in Poincaré map (Fig. 20 (d)). In addition, only the  $f$  and  $3f$  can be observed in frequency spectrum (Fig. 20 (b)), the phase diagram shows a circle in Fig. 20 (c).

## 5. Conclusion

In this paper, a SDOF vehicle suspension model is presented in which the dynamic behaviors of the vehicle vibration system is analyzed with nonlinear spring and damping by using IHBM and NMM. The effects of the damping coefficient  $\zeta$ , excitation amplitude  $F_m$  and excitation frequency  $\Omega$  on the dynamic responses are studied and the conclusions can be summarized as follows:

- (1) The periodic motion of a vehicle nonlinear system are investigated by the IHBM and NMM. The vibration system exhibits period motion, quasi-periodic motion and chaotic behavior in different regions of excitation frequency. The periodic solutions obtained by the IHBM compare very well with those obtained by NMM. In addition, the multi-valued property and hardening type nonlinear behavior of the SDOF vehicle system are observed by amplitude-frequency curves. The transformation of chaotic motion, quasi-periodic motion and periodic motion is also observed.

- (2) For the system, the increase of damping coefficient makes the primary resonance amplitude and spur-harmonic peaks reduce and narrow the range of multi-valued. The motion state is transformed from chaotic motion to periodic motion. In addition, it can be seen from amplitude-frequency curves that when  $\Omega < 0.4$  and  $\Omega > 2.1$ , the changing damping coefficient cannot change vibration amplitude. When  $0.4 < \Omega < 2.1$ , the increase damping coefficient may reduce the amplitude. When the excitation amplitude  $F_m$  is light, the chaotic behavior turns out easily and the spur-harmonic peaks are more obvious. With the decrease of the excitation amplitude, the primary resonance amplitude and spur-harmonic peaks decrease gradually, and the hardening type nonlinear behavior weakens. The multi-valued region narrows down.
- (3) The effect of excitation frequency  $\Omega$  is investigated by NMM. The chaotic motion, quasi-periodic motion and periodic motion of the vehicle system are transformed in a range of different excitation frequencies.

Overall, the SDOF vehicle model presents some complicated vibration characteristics and strong nonlinearity, and a detailed investigation of the dynamic behaviors is provided in this study. In order to study the vibration properties of the vehicle system more deeply, the more accurate multi-degree of freedom vehicle model and some other coupled characteristics of vehicle system need to be taken into consideration. A more precise and reasonable model of the vehicle system will be proposed in further study.

## Acknowledgments

The project was supported by Collaborative Innovation Center of Major Machine Manufacturing in Liaoning; National Support Program, the key common technology research and demonstration of paving equipment for subgrade in alpine (No. 2015BAF07B07); Natural Science Foundation of China (No. 51475084).

## References

- [1] B. Balachandran, E.B. Magrab, *Vibrations*, 2th ed., Cengage Learning, Toronto, 2009.
- [2] S.P. Yang, Y.J. Lu, S.H. Li, An overview on vehicle dynamics, *Int. J. Dyn. Control* 1 (2013) 385–395.
- [3] S. Liang, C.G. Li, Q. Zhu, The influence of parameters of consecutive speed control humps on the chaotic vibration of a 2-DOF nonlinear vehicle model, *J. Vibroeng.* 13 (2011) 406–413.
- [4] F. Liu, S. Liang, Q. Zhu, Q.Y. Xiong, Effects of the consecutive speed humps on chaotic vibration of a nonlinear vehicle model, *ICIC Express Lett.* 4 (2010) 1657–1664.
- [5] J. Zheng, S. Liang, Chaotic vibration of vehicle suspension excited by consecutive speed control hump, *J. Highw. Transp. Res. Dev.* 28 (2011) 132–137.
- [6] S.H. Li, S.P. Yang, W.W. Guo, Investigation on chaotic motion in hysteretic nonlinear suspension system with multi-frequency excitations, *Mech. Res. Commun.* 31 (2004) 229–236.

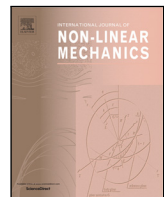
- [7] A.H. Nayfeh, B. Balachandran, *Applied nonlinear dynamics: analytical, computational, and experimental methods*, John Wiley & Sons, Inc., New York, 2006.
- [8] G. Litak, M. Borowiec, M.I. Friswell, Chaotic response of a quarter car model forced by a road profile with a stochastic component, *Chaos, Solitons & Fractals* 39 (2009) 448–456.
- [9] G. Litak, M. Borowiec, M.I. Friswell, Chaotic vibration of a quarter-car model excited by the road surface profile, *Commun. Nonlinear Sci.* 13 (2008) 1373–1383.
- [10] Q. Zhu, M. Ishitobi, Chaos and bifurcations in a nonlinear vehicle model, *J. Sound Vib.* 275 (2004) 1136–1146.
- [11] Q. Zhu, M. Ishitobi, Chaotic vibration of a nonlinear full-vehicle model, *Int. J. Solids Struct.* 43 (2006) 747–759.
- [12] S.J. Zhu, Y.F. Zheng, Y.M. Fu, Analysis of non-linear dynamics of a two-degree-of-freedom vibration system with non-linear damping and non-linear spring, *J. Sound Vib.* 271 (2004) 15–24.
- [13] S. Ikenaga, F.L. Lewis, J. Campos, L. Davis, Active suspension control of ground vehicle based on a full-vehicle model, in: Proceedings of the 2000 American Control Conference (ACC 2000), Chicago, 6 (2000), pp. 4019–4024.
- [14] H.L. Zhang, E.R. Wang, N. Zhang, et al., Semi-active sliding mode control of vehicle suspension with magneto-rheological damper, *Chin. J. Mech. Eng. (Engl.)* 28 (2015) 63–75.
- [15] M. Borowiec, G. Litak, M.I. Friswell, Nonlinear response of an oscillator with a magneto-rheological damper subjected to external forcing, *Appl. Mech. Mater.* 5–6 (2006) 277–284.
- [16] S. Turky, H. Akcay, A study of random vibration characteristics of the quarter-car model, *J. Sound Vib.* 282 (2008) 111–124.
- [17] U. Wagner, On non-linear stochastic dynamics of quarter car models, *Int. J. Non-Linear Mech.* 39 (2004) 753–765.
- [18] G.Q. Wu, Y. Sheng, Review on the application of chaos theory in automobile nonlinear system, *J. Mech. Eng.* 46 (2010) 81–87.
- [19] G. Verros, S. Natsiavas, G. Stepan, Control and dynamics of quarter-car models with dual-rate damping, *J. Vib. Control* 6 (2000) 1045–1063.
- [20] O. Kropáč, P. Múčka, Effect of obstacles in the road profile on the dynamic response of a vehicle, *J. Automob. Eng.* 222 (2008) 353–370.
- [21] B.S. Kim, H.H. Yoo, Ride comfort uncertainty analysis and reliability design of a passenger vehicle undergoing random road excitation, *J. Automob. Eng.* 227 (2013) 433–442.
- [22] Z.Y. Yang, S. Liang, Q. Zhu, Chaotic vibration and comfort analysis of nonlinear full-vehicle model excited by consecutive speed control humps, *Math. Probl. Eng.* 2014 (2014) 1–9.
- [23] Z.Y. Yang, S. Liang, Vibration suppression of four degree-of-freedom nonlinear vehicle suspension model excited by the consecutive speed humps, *J. Vib. Control* 1 (2014) 1–8.
- [24] Y.J. Shen, M. Ahmadian, Nonlinear dynamical analysis on four semi-active dynamic vibration absorbers with time delay, *Shock Vib.* (2013) 649–663.
- [25] M.M. ElMadany, Quadratic synthesis of active controls for a quarter-car model, *J. Vib. Control* 7 (2001) 1237–1252.
- [26] M.M. ElMadany, Dynamic analysis of a slow-active suspension system based on a full car model, *J. Vib. Control* 17 (2011) 39–53.
- [27] Y. Sheng, G.Q. Wu, X.J. Meng, Study on bifurcation, chaos and chaotic control of vehicle suspension with nonlinearities under road excitation, in: Proceedings of the International Conference on Chaotic Modeling, Simulation and Applications (CHAOS2008), Mediterranean Agronom Inst Chania, 2009, pp. 299–308.
- [28] W.W. Yu, X. Guo, Safety and complexity study on vehicle suspension system with hysteretic nonlinearity characteristic under quasi-period multi-frequency excitation, in: Proceedings of the 2011 International Conference on Electronics, Communications and Control (ICECC), Ningbo, 2011, pp. 4497–4500.
- [29] D. Zhuang, F. Yu, Y. Lin, Chaotic threshold analysis of nonlinear vehicle suspension by using a numerical integral method, *Int. J. Automot. Technol.* 8 (2007) 33–38.
- [30] S. Zhong, Y.S. Chen, Bifurcation of piecewise-linear nonlinear vibration system of vehicle suspension, *Appl. Math. Mech.* 30 (2009) 677–684.
- [31] S.W. Lu, Q.F. Jia, W. Yu, X.J. Liu, Nonlinear dynamic characteristics of vehicle suspension system with multi-degrees of freedom, *Chin. J. Appl. Mech.* 2 (2005) 461–465.
- [32] J. Jenny, S. Annika, Nonlinear dynamic behaviour of coupled suspension systems, *Meccanica* 38 (2003) 43–59.
- [33] S. Hamed, R. Mousa, The stability and chaos analysis of a nonlinear wheeled vehicle model under road excitation, in: Proceedings of the ASME 2010 10th Biennial Conference on Engineering Systems Design and Analysis, Istanbul, 6 (2010), pp. 115–120.
- [34] C.B. Ren, J.L. Zhou, Periodic solution and stability analysis for piecewise coupled system, *Chin. J. Appl. Mech.* 28 (2011) 527–531.
- [35] M. Javad, K. Ahmad, Chaotic vibrations of a nonlinear air 8suspension system under consecutive half sine speed bump, *Indian J. Sci. Technol.* 8 (2015) 72–84.
- [36] M. Borowiec, G. Litak, Transition to chaos and escape phenomenon in two-degrees-of-freedom oscillator with a kinematic excitation, *Nonlinear Dyn.* 70 (2012) 1125–1133.
- [37] Y. Sheng, G.Q. Wu, Quantitative study of automotive nonlinear suspension system based on incremental harmonic balance method, *J. Tongji Univ.* 39 (2011) 405–410.

Update

**International Journal of Non-Linear Mechanics**

Volume 109, Issue , March 2019, Page 213

DOI: <https://doi.org/10.1016/j.ijnonlinmec.2018.12.010>



## International Journal of Non-Linear Mechanics

journal homepage: [www.elsevier.com/locate/nlm](http://www.elsevier.com/locate/nlm)

## Corrigendum

## Corrigendum to “Nonlinear dynamic analysis of a quarter vehicle system with external periodic excitation” [Int. J. Non-Linear Mech. 84 (2016) 82–93]

Shihua Zhou, Guiqiu Song\*, Mengnan Sun, Zhaohui Ren

School of Mechanical Engineering &amp; Automation, Northeastern University, Shenyang, 110819 Liaoning, People's Republic of China

The authors regret Modify the Fig. 5.

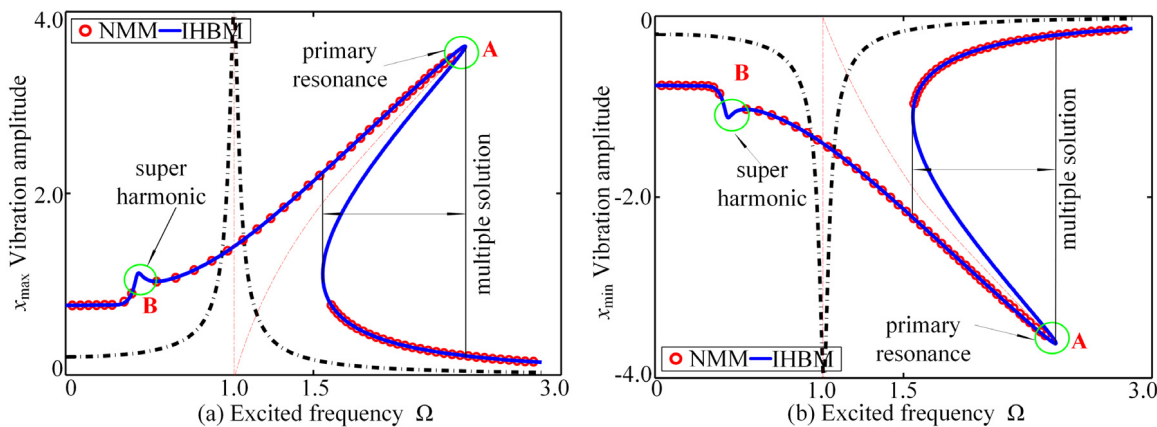


**Fig. 5.** Comparison between IHBM and NMM. **O** NMM, **—** IHBM. (For interpretation of the references to colour in this figure legend, the reader is referred to the web version of this article.)

The authors would like to apologise for any inconvenience caused.

DOI of original article: <https://doi.org/10.1016/j.ijnonlinmec.2016.04.014>.

\* Corresponding author.

E-mail address: [guiqiusong@126.com](mailto:guiqiusong@126.com) (G. Song).